Volumetric imaging of holographic optical traps

Yohai Roichman, Ilias Cholis, and David G. Grier
Department of Physics and Center for Soft Matter Research, New York University, 4 Washington Place, New York, NY 10003

The holographic optical trapping technique creates arbitrary three-dimensional configurations of optical traps, each with individually specified characteristics. Holographic modification of the individual traps' wavefronts can transform conventional point-like optical tweezers into traps with different structures and properties, and can position them independently in three dimensions. Here, we describe a technique for rapidly characterizing holographic optical traps' three-dimensional intensity distributions. We create volumetric representations by by holographically translating the traps through the optical train's focal plane, acquiring a stack of two-dimensional images in the process. We apply this technique to holographic line traps, which are used to create tailored one-dimensional potential energy landscapes for mesoscopic objects. These measurements highlight problems that can arise when projecting extended traps with conventional optics and demonstrates the effectiveness of shape-phase holography for creating nearly ideal line traps.

A single-beam optical trap uses forces exerted by focused beam of light to confine a small object to a particular point in space. Commonly known as optical tweezers [1], these optical micromanipulators have revolutionized research in several branches of biology, chemistry and physics. Extended optical tweezers, which sometimes are called line traps, differ from point-like optical tweezers by acting as one-dimensional potential energy landscapes for mesoscopic objects. Line traps can be used to rapidly screen the interactions between colloidal particles and biological materials [2–4] and thus have potentially valuable applications in biological research, medical diagnostics and drug discovery. These applications, however, require methods for projecting line traps with precisely specified characteristics. Recently, we introduced a class of extended optical traps created with shape-phase holography [5] whose intensity and phase profiles can be independently specified. In this article, we provide a detailed view of these traps' three-dimensional intensity distributions and contrast their performance with other classes of extended optical traps.

Our method is based on the optimized holographic trapping technique [6, 7], shown schematically in Fig. 1. Here, a beam of light from a frequency-doubled solid-state laser (Coherent Verdi) operating at a wavelength of $\lambda = 532$ nm is directed to the input pupil of a high-numerical-aperture objective lens (Nikon 100× Plan Apo, NA 1.4, oil immersion) that focuses it into an optical trap. The laser beam is imprinted with a phase-only hologram by a computer-addressed liquid-crystal spatial light modulator (SLM, Hamamatsu X8267 PPM) in a plane conjugate to the objective's input plane. As a result, the light field, $\psi(\boldsymbol{r})$, in the objective's focal plane is related to the field $\psi(\boldsymbol{\rho})$ in the plane of the SLM by the Fraunhofer transform [8]

$$\psi(\boldsymbol{r}) = -\frac{i}{\lambda f} \int_\Omega \psi(\boldsymbol{\rho}) \exp\left(-i \frac{2\pi}{\lambda f} \boldsymbol{r} \cdot \boldsymbol{\rho}\right) d^2\rho, \qquad (1)$$

where f is the objective's focal length, where Ω is the optical train's aperture, and where we have dropped irrelevant phase factors. Assuming that the laser illuminates the SLM with a radially symmetric amplitude profile, $u(\rho)$, and uniform phase, the field in the SLM's plane may be written as

$$\psi(\boldsymbol{\rho}) = u(\rho) \exp(i\varphi(\boldsymbol{\rho})), \qquad (2)$$

where $\varphi(\boldsymbol{\rho})$ is the real-valued phase profile imprinted on the beam by the SLM. The SLM in our system imposes phase shifts between 0 and 2π radians at each pixel of a 768×768 array. This two-dimensional phase array can be used to project a computer-generated phase-only hologram, $\varphi(\boldsymbol{\rho})$, designed [7] to transform the single optical tweezer into any desired three-dimensional configuration of optical traps, each with individually specified intensities and wavefront properties.

Ordinarily, the pattern of holographic optical traps would be put to use by projecting it into a fluid-borne sample mounted in the objective's focal plane. To characterize the light field, we instead mount a front-surface mirror in the sample plane. This mirror reflects the trapping light back into the objective lens, which transmits

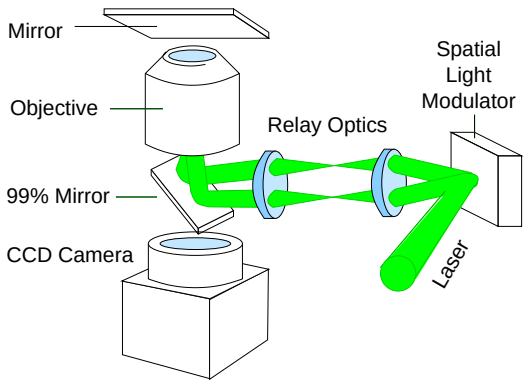

FIG. 1: Projecting extended optical traps with computer generated holograms.

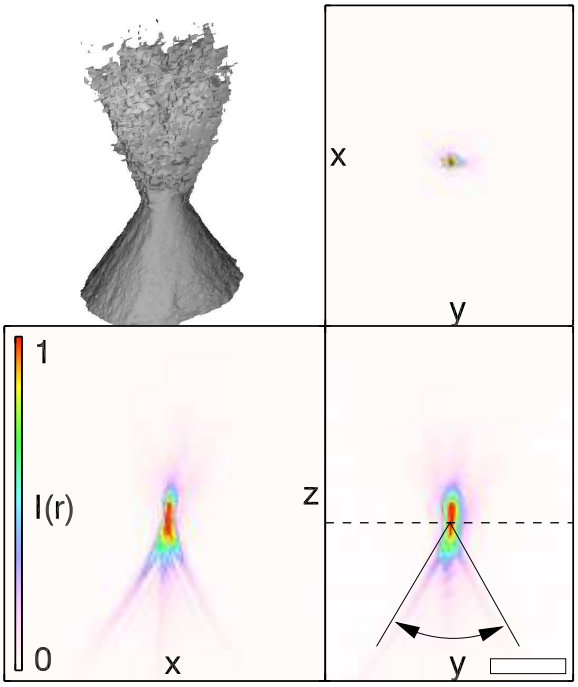

FIG. 2: Three-dimensional reconstruction of an optical tweezer propagating along the z axis. Cross-sections in the xy, yz and xz planes are colored by intensity according to the inset scale. The horizontal dashed line indicates the plane $z = z_0$ in which the xy section is obtained. The inset isosurface encloses 95 percent of the incident light and the scale bar denotes 5 μm.

images of the traps through a partially reflecting mirror to a charge-coupled device (CCD) camera (NEC TI-324AII). In our implementation, the objective, camera and camera eyepiece are mounted in a conventional optical microscope (Nikon TE-2000U).

Three-dimensional reconstructions of the optical traps' intensity distribution can be obtained by translating the mirror relative to the objective lens. Equivalently, the traps can be translated relative to the fixed mirror by superimposing the parabolic phase function

$$\varphi_z(\boldsymbol{\rho}) = -\frac{\pi\rho^2 z}{\lambda f^2}, \tag{3}$$

onto the hologram $\varphi_0(\boldsymbol{\rho})$ encoding a particular pattern of traps. The combined hologram, $\varphi(\boldsymbol{\rho}) = \varphi_0(\boldsymbol{\rho}) + \varphi_z(\boldsymbol{\rho}) \bmod 2\pi$, projects the same pattern of traps as $\varphi_0(\boldsymbol{\rho})$ but with each trap translated by $-z$ along the optical axis. The resulting image obtained from the reflected light represents a cross-section of the original trapping intensity at distance z from the objective's focal plane. Translating the traps under software control is particularly convenient because it minimizes changes in the optical train's properties due to mechanical motion and facilitates more accurate displacements along the optical axis. Images obtained at each value of z are stacked up to yield a complete volumetric representation of the intensity distribution.

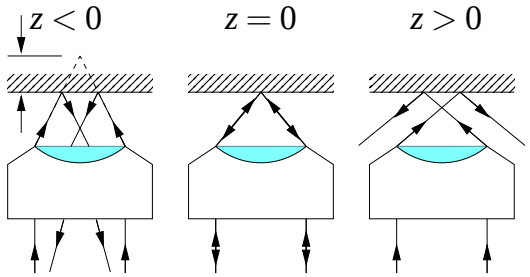

FIG. 3: Virtually all of the light focused by the objective lens onto the mirror is collected for $z \leq 0$. For $z > 0$, by contrast, the outermost rays fall outside the objective's pupil, reducing the overall collection efficiency. This figure also indicates the sign convention for z.

As shown schematically in Fig. 3, the objective captures essentially all of the reflected light for $z \leq 0$. For $z > 0$, however, the outermost rays of the converging trap are cut off by the objective's output pupil, and the contrast is reduced accordingly. This could be corrected by multiplying the measured intensity field by a factor proportional to z for $z > 0$. The appropriate factor, however, is difficult to determine accurately, so we present only unaltered results.

Figure 2 shows a conventional optical tweezer reconstructed in this way and displayed as an isointensity surface at 5 percent peak intensity and in three cross-sections. The former representation is useful for showing the overall structure of the converging light, and the cross-sections provide an impression of the three dimensional light field that will confine an optically trapped object. The angle of convergence of 63° in immersion oil obtained from these data is consistent with an overall numerical aperture of 1.4. The radius of sharpest focus, $r_{\min} \approx 0.2$ μm, is consistent with diffraction-limited focusing of the beam.

These results highlight two additional aspects of this reconstruction technique. The objective lens is designed to correct for spherical aberration when light passing through water is refracted by a glass coverslip. Without this additional refraction, the projected optical trap actually is degraded by roughly 20λ of spherical aberration, introduced by the lens. This reduces the apparent numerical aperture and also extends the trap's focus along the $\hat{\boldsymbol{z}}$ axis. The trap's effective numerical aperture in water would be roughly 1.2. The effect of spherical aberration can be approximately corrected by pre-distorting the beam with the additional phase profile

$$\varphi_a(\boldsymbol{\rho}) = \frac{a}{\sqrt{2}}\left(6x^4 - 6x^2 + 1\right), \tag{4}$$

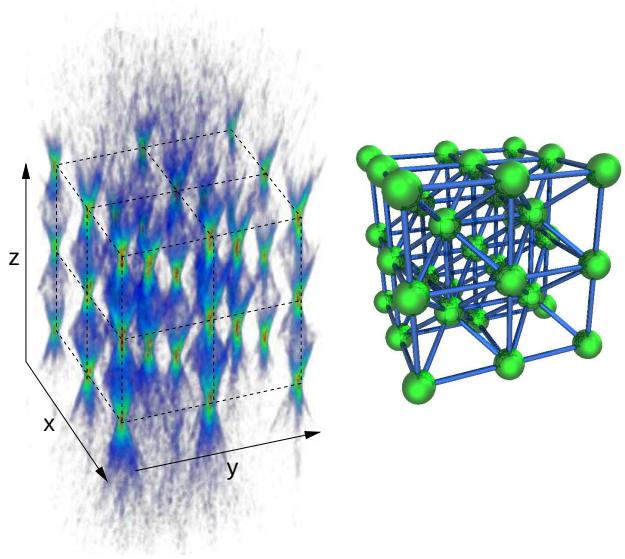

FIG. 4: Volumetric reconstruction of 35 optical tweezers arranged in a body-centered cubic lattice, shown schematically on the right.

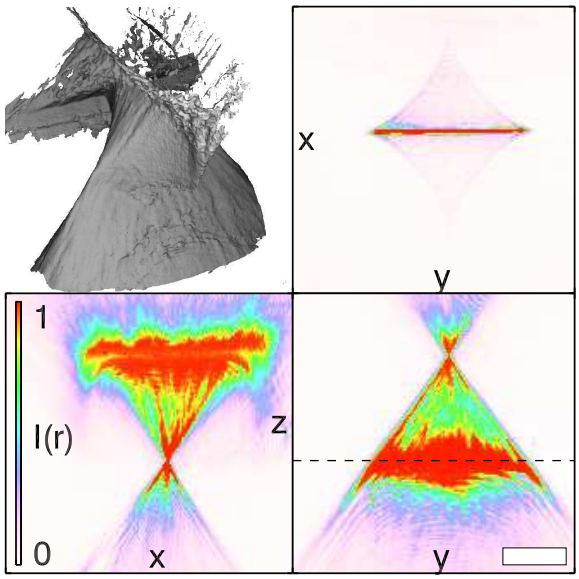

FIG. 5: Reconstruction of a cylindrical lens line tweezer.

the Zernike polynomial describing spherical aberration [9]. The radius, x, is measured as a fraction of the optical train's aperture, and the coefficient a is measured in wavelengths of light. This procedure is used to correct for small amount of aberration present in practical optical trapping systems to optimize their performance [7, 10].

This correction was applied to the array of 35 optical tweezers shown as a three-dimensional reconstruction in Fig. 4. These optical traps are arranged in a three-dimensional body-centered cubic (BCC) lattice with a 10.8 μm lattice constant. Without correcting for spherical aberration, these traps would blend into each other along the optical axis. With correction, their axial intensity gradients are clearly resolved. This accounts for holographic traps' ability to organize objects along the optical axis [11, 12].

Correcting for aberrations reduces the range of displacements, z, that can be imaged. Combining $\varphi_a(\boldsymbol{\rho})$ with $\varphi_z(\boldsymbol{\rho})$ and $\varphi_0(\boldsymbol{\rho})$ increases gradients in $\varphi(\boldsymbol{\rho})$, particularly for larger values of ρ near the edges of the DOE. Diffraction efficiency falls off rapidly when $|\nabla\varphi(\boldsymbol{\rho})|$ exceeds $2\pi/\Delta\rho$, the maximum phase gradient that can be encoded on an SLM with pixel size $\Delta\rho$. This problem is exacerbated when $\varphi_0(\boldsymbol{\rho})$ itself has large gradients. We therefore study more complex trapping patterns without aberration correction. In particular, we use uncorrected volumetric imaging to illustrate the comparative advantages of extended optical traps created by recently introduced holographic techniques.

Extended optical traps have been projected in a time-shared sense by rapidly scanning a conventional optical tweezer along the trap's intended contour [2–4, 13–15]. A scanned trap has optical characteristics as good as a point-like optical tweezer, and an effective potential energy well that can be tailored by adjusting the instantaneous scanning rate. Kinematic effects due to the trap's motion can be minimized by scanning rapidly enough [14]. For some applications, however, continuous illumination or the simplicity of an optical train with no scanning capabilities can be desirable.

Continuously illuminated line traps have been created by expanding an optical tweezer along one direction. This can be achieved, for example, by introducing a cylindrical lens into the objective's input plane [16, 17]. Equivalently, a cylindrical-lens line tweezer can be implemented by encoding the function $\varphi_c(\boldsymbol{\rho}) = \pi\, z_0\, \rho_x^2/(\lambda f^2)$ on the SLM [18]. The result, shown in Fig. 5 appears serviceable in the plane of best focus, $z = z_0$, with the point-like tweezer having been extended to a line with nearly parabolic intensity and a nearly Gaussian phase profile. The three-dimensional reconstruction in Fig. 5, however, reveals that the cylindrical lens merely introduces a large amount of astigmatism into the beam, creating a second focal line perpendicular to the first. This is problematic because the astigmatic beam's axial intensity gradients are far weaker than a conventional optical tweezer's. Consequently, cylindrical-lens line traps typically cannot localize objects against radiation pressure along the optical axis.

Replacing the single cylindrical lens with a cylindrical Keplerian telescope [17] eliminates the astigmatism and thus creates a stable three-dimensional optical trap. Similarly, using an objective lens to focus two interfering beams creates an interferometric optical trap capable of

three-dimensional trapping [19, 20]. These approaches, however, offer little control over the extended traps' intensity profiles, and neither affords control over the phase profile.

Shape-phase holography provides absolute control over both the amplitude and phase profiles of an extended optical trap at the expense of diffraction efficiency. It also yields traps with optimized axial intensity gradients, suitable for three-dimensional trapping [5]. If the line trap is characterized by an amplitude profile $\tilde{u}(\rho_x)$ and a phase profile $\tilde{p}(\rho_x)$ along the $\hat{\boldsymbol{\rho}}_{\boldsymbol{x}}$ direction in the objective's focal plane, then the field in the SLM plane is given by Eq. (1) as

$$\psi(\boldsymbol{\rho}) = u(\rho_x)\, \exp(ip(\rho_x)), \tag{5}$$

where the phase $p(\rho_x)$ is adjusted so that $u(\rho_x) \geq 0$. Shape-phase holography implements this one-dimensional complex wavefront profile as a two-dimensional phase-only hologram [5]

$$\varphi(\boldsymbol{\rho}) = \begin{cases} p(\rho_x), & \boldsymbol{\rho} \in S(\boldsymbol{\rho}) \\ q(\boldsymbol{\rho}), & \boldsymbol{\rho} \notin S(\boldsymbol{\rho}) \end{cases}, \tag{6}$$

where the shape function $S(\boldsymbol{\rho})$ allocates a number of pixels along the row ρ_y proportional to $u(\rho_x)$. One particularly effective choice is for $S(\boldsymbol{\rho})$ to select pixels randomly along each row in the appropriate relative numbers [5]. The unassigned pixels then are given values $q(\boldsymbol{\rho})$ that redirect the excess light away from the intended line. Typical results are presented in Fig. 6.

Unlike the cylindrical-lens trap, the holographic line trap focuses as a conical wedge to a single diffraction-limited line in the objective's focal plane. Consequently, its transverse angle of convergence is comparable to that of an optimized point trap. This means that the holographic line trap has comparably strong axial intensity gradients, which explains its ability to trap objects stably against radiation pressure in the $\hat{\boldsymbol{z}}$ direction.

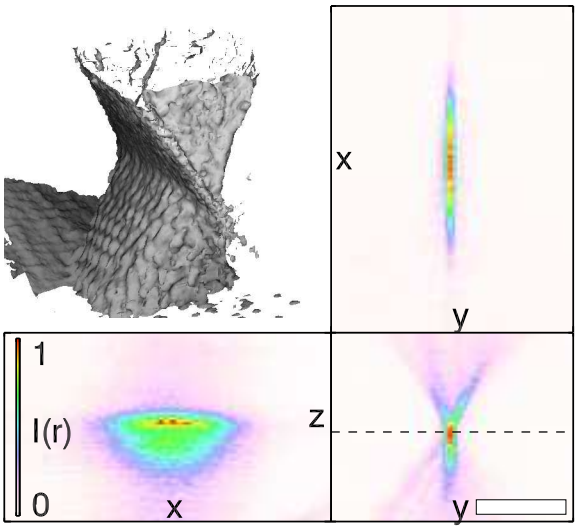

FIG. 6: Three-dimensional reconstruction of a holographic optical line trap featuring diffraction-limited convergence to a single focal plane.

The line trap's transverse convergence does not depend strongly on the choice of intensity profile along the line. Its three-dimensional intensity distribution, however, is very sensitive to the phase profile along the line. Abrupt phase changes cause intensity fluctuations through Gibbs phenomenon. Smoother variations do not affect the intensity profile along the line, but can substantially restructure the beam. The line trap created by a cylindrical lens, for example, has a parabolic phase profile. Inserting this choice into Eq. (2) and calculating the associated shape-phase hologram with Eqs. (1) and (6) yields the same cylindrical lens phase profile. This observation opens the door to applications in which the phase profile along a line can be tuned to create a desired three-dimensional intensity distribution, or in which the measured three-dimensional intensity distribution can be used to assess the phase profile along the line. These applications will be discussed elsewhere.

This work was supported by the National Science Foundation through grant number DMR-0451589.

[1] A. Ashkin, J. M. Dziedzic, J. E. Bjorkholm, and S. Chu, Opt. Lett. **11**, 288 (1986).
[2] R. Verma, J. C. Crocker, T. C. Lubensky, and A. G. Yodh, Phys. Rev. Lett. **81**, 4004 (1998).
[3] J. C. Crocker, J. A. Matteo, A. D. Dinsmore, and A. G. Yodh, Phys. Rev. Lett. **82**, 4352 (1999).
[4] R. Verma, J. C. Crocker, T. C. Lubensky, and A. G. Yodh, Macromolecules **33**, 177 (2000).
[5] Y. Roichman and D. G. Grier, Opt. Lett. **31**, 1675 (2006).
[6] E. R. Dufresne and D. G. Grier, Rev. Sci. Instrum. **69**, 1974 (1998).
[7] M. Polin, K. Ladavac, S.-H. Lee, Y. Roichman, and D. G. Grier, Opt. Express **13**, 5831 (2005).
[8] J. W. Goodman, *Introduction to Fourier Optics* (McGraw-Hill, New York, 1996), 2nd ed.
[9] M. Born and E. Wolf, *Principles of Optics* (Cambridge University Press, Cambridge, 1999), 7th ed.
[10] Y. Roichman, A. S. Waldron, E. Gardel, and D. G. Grier, Appl. Opt. **45**, 3425 (2005).
[11] J. Liesener, M. Reicherter, T. Haist, and H. J. Tiziani, Opt. Commun. **185**, 77 (2000).
[12] Y. Roichman and D. G. Grier, Opt. Express **13**, 5434 (2005).
[13] K. Sasaki, M. Koshio, H. Misawa, N. Kitamura, and H. Masuhara, Opt. Lett. **16**, 1463 (1991).
[14] L. P. Faucheux, L. S. Bourdieu, P. D. Kaplan, and A. J. Libchaber, Phys. Rev. Lett. **74**, 1504 (1995).
[15] L. P. Faucheux, G. Stolovitzky, and A. Libchaber, Phys. Rev. E **51**, 5239 (1995).
[16] T. Yu, F.-C. Cheong, and C.-H. Sow, Nanotechnology

15, 1732 (2004).
[17] P. L. Biancaniello, A. J. Kim, and J. C. Crocker, Phys. Rev. Lett. **94**, 058302 (2005).
[18] K. J. Moh, W. M. Lee, W. C. Cheong, and X.-C. Yuan, Appl. Phys. B **80**, 973 (2005).
[19] A. E. Chiou, W. Wang, G. J. Sonek, J. Hong, and M. W. Berns, Opt. Commun. **133**, 7 (1997).
[20] E. Schonbrun, R. Piestun, P. Jordan, J. Cooper, K. D. Wulff, J. Courtial, and M. Padgett, Opt. Express **13**, 3777 (2005).